World Electric Vehicle Journal

MDPI

Article

Optimal Design of a Short Primary Double-Sided Linear Induction Motor for Urban Rail Transit

Hanming Wang, Jinghong Zhao *, Yiyong Xiong *, Hao Xu and Sinian Yan

School of Electrical Engineering, Naval University of Engineering, Wuhan 430030, China; wanghanmingcsw@outlook.com (H.W.); xuhao10141205@163.com (H.X.); ysnian0504@126.com (S.Y.)
* Correspondence: zm.wang868@mails.ccnu.edu.cn (J.Z.); 6110116146@email.ncu.edu.cn (Y.X.)

Abstract: Linear induction motors (LIMs) have been widely used in rail transit. However, Due to the breaking of the primary core and the large air gap, the efficiency and power factor of LIMs are seriously damaged, causing a large amount of energy waste. To improve the efficiency and power factor of LIMs for urban rail transit, we present a new optimization method for the design of a short primary double-sided linear induction motor (SP-DLIM) with a rated speed of 45 km/h and small thrust. The method is based on a steady state equivalent circuit model and the differential evolutionary algorithm (DEA). Moreover, the design constraints and the objective functions are proposed for the optimization problem. Finally, the optimized SP-DLIM is simulated by 2D transient finite element method (FEM). The 2-D transient FEM results verify the accuracy of the optimization method proposed in this paper.

Keywords: linear induction motor; rail transit; design optimization; differential evolutionary algorithm

Citation: Wang, H.; Zhao, J.; Xiong, Y.; Xu, H.; Yan, S. Optimal Design of a Short Primary Double-Sided Linear Induction Motor for Urban Rail Transit. *World Electr. Veh. J.* **2022**, *13*, 30. https://doi.org/10.3390/wevj13020030

Academic Editors: Fanlin Meng and Xinan Yang

Received: 19 December 2021
Accepted: 19 January 2022
Published: 31 January 2022

1. Introduction

Linear induction motors (LIMs) have been used in rail transit such as maglev vehicles, air bus and other urban applications [1–8]. Specifically, maglev systems have been successfully built in several countries all over the world, and can reach a maximum speed of 600 km/h, which greatly benefits to people's travel. Additionally, air bus is gradually being applied as a means to reduce the pressure of urban ground congestion with a significant advantage of needing less space [8]. As the propulsion system of the above applications, LIMs have many advantages such as simple structure, low cost, small swerving radius, non-adhesion drive and strong climbing capability, et al. However, the shortcomings of linear induction motors cannot be ignored. First, in order to ensure that the stator core and mover do not collide during operation, LIMs always have large air-gap length compared with that of rotated induction machines, therefore the efficiency and power factor of LIMs are severely reduced. Second, due to the core breaking, LIMs are affected by the end effect phenomenon [1,9–11], which further decreases the performance of LIMs. For rail transit, such high-power and continuous-running electrical equipment, minor shortcomings may also cause huge energy waste over time. Thus, it is essential to optimize the performance of LIMs in design.

The design of LIMs includes various parameters. Changing one parameter may have the opposite effect and different sensitivity on different output characteristics. Therefore, the optimal design of LIMs is a comprehensive problem considering different outputs as objectives. Many researches have been conducted on the optimization design of LIMs. Osawa S. et al. [12] decreased the primary weight of LIMs. Laporte B et al. [13] investigated the optimization of winding design in LIMs. Isfahani et al. [14] applied genetic algorithm (GA) to enhance the efficiency and the power factor of a single-sided LIM (SLIM). The optimization is effective, however, only the only the primary current density, primary width to pole pitch ratio, and secondary aluminum sheet thickness have been chosen as design parameters. Other main parameters of LIMs are not included. Lucas C et al. [15]

applied an imperialist competitive algorithm to the optimization model of LIM presented by Isfahani. Bazghaleh et al. [16] considered the end effect in the equivalent circuit of the LIM, and proposed a new method for suppressing end effect. Bazghaleh et al. [17] investigated the application of PSO for optimizing high-speed single-sided linear induction motors. Zhao et al. [18] employed the GA to optimize the efficiency and power factor of a high-temperature superconducting linear induction motor. Shiri et al. [19] optimized a high-speed (288 km/h) single-sided linear induction motor and proposed a method to weaken the end effect braking force.

Although some researches have been done on the optimal design of linear induction motors, most of the researches are on the single-sided linear induction motors (SLIMs), seldom researchers study the optimal design of double-sided linear induction motors (DLIMs). Moreover, the investigations on optimal design of medium-high speed LIMs are still insufficient. Medium-high speed LIMs are the main propulsion system of urban transit, therefore, optimizing medium-high speed linear induction motors is of great significance to the development of urban rail transit. Figure 1 shows the conceptual diagram of SP-DLIM as the propulsion system of urban rail transit.

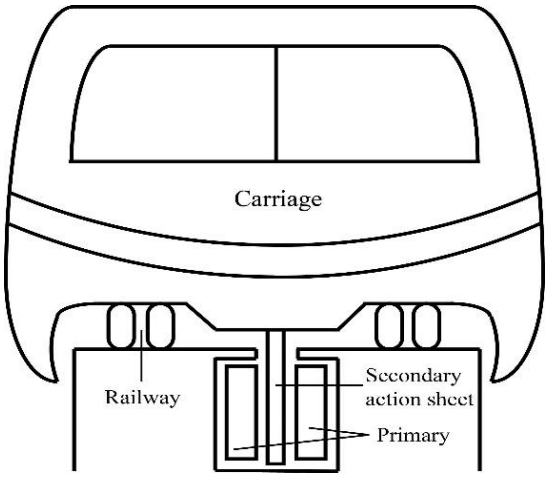

Figure 1. Schematic diagram of the SP-DLIM-driven urban rail transit.

This article studies the optimal design method of a short-primary double-sided linear induction motor (SP-DLIM) with a rated speed of 45 km/h and rated thrust of 1000 N, adopting a steady state equivalent circuit considering both transverse and longitudinal end effect [1]. In the equivalent circuit mathematical model, the influence of the end effect is expressed by four correction coefficients. With the equivalent circuit, the output characteristics including efficiency, power factor, and the thrust can be calculated by design parameters (structural parameters and electrical power supply parameters). Therefore, once the main constraints and boundary values of design parameters are given, the outputs can be calculated. What's more, the objective function is properly defined to optimize the outputs. The design optimization process is to obtain the parameters that can provide superior output characteristics within the predefined search range. Further, differential evolutionary algorithm (DEA) is applied to optimize the design. The optimal machine is simulated by 2-D transient finite element method (FEM) to verify the validation of the optimization method. Further, the main contributions of the paper are as follows:

First, a new optimization method of a low-medium speed and double-sided linear induction motor (DLIM) for urban transit is proposed. The proposed optimization method considers primary current, and constraints the input voltage within a certain range.

Second, a steady state equivalent circuit that takes into account both longitudinal and transverse end effect is introduced in the optimization model.

Third, differential evolutionary algorithm is applied to deal with the double-sided linear induction motor (DLIM) optimization problem.

The 2-D finite element method (FEM) verifies the accuracy of the optimization method. Therefore, this method can provide reference for the optimization design of linear induction motors and various electric vehicles (EVs) in smart grids.

2. Equivalent Circuit of the Short Primary Double-Sided Linear Induction Motor

Long et al. [9], Xu et al. [20], Lv et al. [21], Ma et al. [1] and Yang et al. [22,23] have derived and analyzed the equivalent circuit mathematical model of the linear induction motors (LIMs), based on a method of equal complex power of magnetic field and circuit. Among them, Long et al. [9] have conducted the researches on the short primary double-sided linear induction motors (SP-DLIMs). The physical model of a SP-DLIM is shown in the Figure 2. 2a is the primary stack width, 2c is the width of secondary sheet, b_s represents slot width, t_s is the tooth width, τ_s is slot pitch, h_1 denotes slot height, d is the thickness of the secondary action sheet, g is the length between the surface of two primary cores, l_ce is the length of the end connection of the primary winding per phase, and v_x is the mechanical speed of the secondary plate.

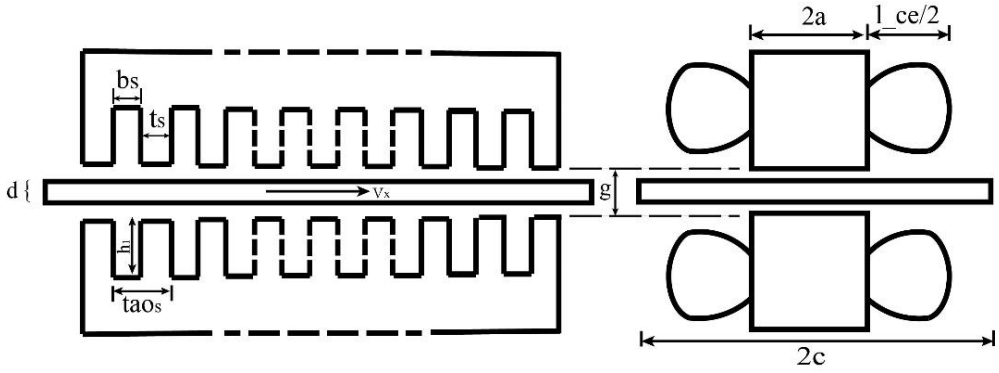

Figure 2. Structure of a SP-DLIM.

This section established an equivalent circuit mathematical model of SP-DLIMs, and the expressions of essential outputs are derived. The purpose of establishing the equivalent circuit mathematical model is to calculate the output characteristics only through the design parameters. The equivalent circuit model is illustrated as Figure 3. Importantly, the expressions of all parameters in the equivalent circuit are as follows.

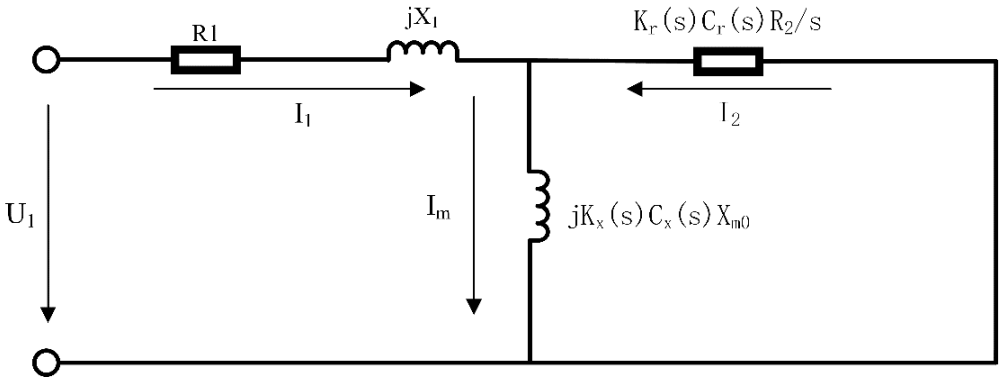

Figure 3. Equivalent circuit of the SP-DLIM.

The primary winding resistance can be expressed as follows [14]:

$$R_1 = \frac{J_c}{\sigma_{cu}} \frac{(4a + 2l_{ce})}{N_{ph} I_{ph}} N_{ph}^2 \quad (1)$$

where J_c is the primary current density (A/m^2) , a is the half of the primary stack width. l_{ce} represents the length of the primary turn's end connection per phase, N_{ph} denotes the number of turns per phase, and σ_{cu} is the conductivity of the conductors.

The primary inductance with a single layer full pitch winding is expressed as [9]:

$$X_1 = 15.8\frac{f_1}{100}\left(\frac{N_{ph}}{100}\right)^2\frac{2a}{q}\left(\frac{\lambda_s+\lambda_t+\lambda_d+\lambda_e}{p}\right) \tag{2}$$

where f_1 is the supply frequency, q is the number of slots per pole per phase, p is the number of pole pairs. Further, λ_s, λ_t, λ_d and λ_e represents the slot leakage permeance, tooth leakage permeance, harmonic leakage permeance and end connection leakage permeance, respectively, which are referred to [9].

The slot leakage permeance is as follows:

$$\lambda_s = \frac{h_1}{3b_s} + \frac{0.05h_1}{b_s} \tag{3}$$

where b_s is slot width, h_1 is slot height and h_0 is slot open height. Notably, $0.05\,h_1$ is the predefined slot open height in this paper, which can be selected based on different requirements.

Tooth leakage permeance is formulated as:

$$\lambda_t = \frac{5g}{10b_s + 4g} \tag{4}$$

where g is the mechanical air gap length between two primaries.

Harmonic leakage permeance is given by:

$$\lambda_d = \frac{t_s k_{w1}^2}{12g_e}\cdot\left[1+k_\beta\left(\frac{m_1 q}{5}\right)^2\right] \tag{5}$$

where t_s is primary tooth width, k_{w1} is the winding's factor, g_e is equivalent air gap length, and the coefficient k_β can be looked up from the handbooks of rotated induction motors, which is set to 0.0644 in this article. Further, m_1 denotes the number of phases, and q is the number of slots per pole per phase.

End connection leakage permeance is expressed as:

$$\lambda_e = 0.34\frac{q}{2a}(l_{ce} - 0.64\beta_y\tau)k_y^2 \tag{6}$$

where a denotes half of the primary stack width, l_{ce} is the length of end connection per phase of the primary winding, τ is the pole pitch, and k_y is the short-pitch factor, which can be calculated with reference to the theory of rotating electrical machines as follows:

$$k_y = \sin(\frac{\pi}{2}\beta_y) \tag{7}$$

$$\beta_y = \frac{sp}{m_1 q} \tag{8}$$

where sp is winding pitch. What's more, For the single-layer full-pitch winding set in this article, $\beta_y = k_y = 1$.

The secondary resistance referred to the primary is expressed as [9,23]:

$$\frac{R_2{}'}{s} = \frac{4am_1(N_1k_{w1})^2}{\sigma_{Al}dp\tau s} \tag{9}$$

where N_1 is the number of turns per phase, σ_{Al} is the conductivity of aluminum, and d is the thickness of the secondary plate.

The magnetizing reactance is as follows [9,23]:

$$x_{m0} = \frac{4\mu_0 a m_1 v_s (N_1 k_{w1})^2}{p g_e \pi} \tag{10}$$

Equivalent air gap length (g_e) can be modified based on mechanical gap length (g) by two coefficients. One is the Carter's factor, another is the fringing coefficient. The fringing coefficient may be considered because the magnetic airgap to per pole pitch ratio of SP-DLIMs is much larger than that of rotary induction motors [10].

$$g_e = k_c k_g g \tag{11}$$

Moreover, the end effect factor K_r, K_x, C_r, C_x can be referred to the literature [23].

Then, the output thrust can be calculated as:

$$F_{em} = \frac{m_1 {I_2}^2 R_2 K_r C_r}{v_s s} \tag{12}$$

where v_s represents the synchronous speed, which can be derived from the synchronous speed of the rotated induction machine, formulated as:

$$v_s = 2\tau f \tag{13}$$

It should be noted that for linear induction motors with large air gap length, the secondary heat loss can be ignored, but not for induction machines with small airgap length. Moreover, in this paper, the iron loss is ignored as well.

Embodying the ratio of output power to the total active power, nominal efficiency is given by:

$$\eta = \frac{F_{em} v_x}{F_{em} v_s + m_1 {I_1}^2 R_1} \tag{14}$$

The power factor is formulated as:

$$PF = \frac{m_1 {I_1}^2 R_1 + F_{em} v_s}{m_1 I_1 U_1} \tag{15}$$

It reflects the active power to the total input power ratio. And the product of efficiency and power factor is the ratio of output power to the input.

Where

$$I_1 = \frac{\pi {d_{con}}^2}{4} Jc \tag{16}$$

$$U_1 = |R_1 + jX_1 + Z_2| I_1 \tag{17}$$

$$I_2 = abs\left(\frac{U_1 - I_1 (R_1 + \mathrm{j}X_1)}{\frac{K_r C_r R_2'}{s}} \right) \tag{18}$$

$$Z_2 = \frac{1}{\frac{s}{K_r C_r R_2'} + \frac{1}{j K_x C_x x_{m0}}} \tag{19}$$

Based on the above analytical model, the objective function can be defined. The objective function can provide a guide for optimizing the performance of linear induction machine. The objective function for optimizing the efficiency, power factor and weight of the machine is established as follows:

$$\text{Objective function} = \frac{\eta \cdot pf \cdot F_{em}}{weight} \tag{20}$$

As the numerator increases, the denominator decreases, that is, the efficiency and power factor increase, and the motor weight reduces, then the objective function value increases. Thus, the motor optimization process can be transformed into a process to maximize the value of the objective function.

3. Design Optimization Process

Based on the above mathematical model, we utilize differential evolutionary (DE) algorithm [24] to optimize the design of SP-DLIM. The 11 design parameters to be optimized are primary stack width ($2a$), the ratio of slot width to slot pitch (b_s/τ_s), wire diameter (d_{con}), airgap length (g), secondary thickness (d), slip (s), primary current density (Jc), power frequency (f_1), number of pole pairs (p), number of slots per pole per phase (q), and number of turns per slot (Nz). This chapter introduces the main indicators, search range of parameters, constraints and the optimization process of the optimal design.

3.1. Main Indicators of SP-DLIM

Usually, the design optimization of the electrical machine is based on the required output power (force and velocity for SP-DLIM). Therefore, guided by previous works [1–3], some of the indicators of a SP-DLIM with low-medium speed and small thrust are displayed as Table 1:

Table 1. Main indicators of SP-DLIM.

Line Voltage	500 V
Rated thrust	1.1 kN ± 5%
Rated speed	45 Km/h
Winding layer	1

3.2. Parameter Search Range of the Optimal Design

Differential evolutionary (DE) algorithm is employed to optimize the design of SP-DLIM. However, the most critical part is how to apply the algorithm to the design optimization. The usual practice is to include the initial design parameters in the population. Then, DE updates the population to obtain a better objective function value through three strategies, namely mutation, crossover and selection.

The essential technics of DE are as follows:

3.2.1. Initialization

To work out the design optimization problem of DLIM, first, the solution vectors must be created. In each solution vector, there are total D variables corresponding to D design parameters. Specifically, there are 11 design parameters with different boundary ranges in this paper, therefore, the solution vectors are initialized as follows:

$$X_{i,j}^{ini} = lb_j + rand \cdot (ub_j - lb_j) \tag{21}$$

where I denotes the i-th solution vector, j indicates the j-th variable in a solution vector. lb_j and ub_j represent the lower bound and upper bound of the j-th variable. Then, solution vectors execute the DE operation to update.

3.2.2. Mutation

One of the most efficient mutation strategies "DE/rand/1" is applied in this paper, which is expressed as follows:

$$V_i^G = X_{r1}^G + rand \cdot (X_{r2}^G - X_{r3}^G) \tag{22}$$

where ${V_i}^G$ is the i-th newly generated solution vector in the G-th generation, which concludes all the design parameters that are randomly preset in the search range, $i \in [1, NV]$. X is the current population in the G-th generation. NV represents the number of total vectors in every iteration. "$r1$, $r2$, $r3$" denote three different integers with different values of i. What's more, the search range will be proposed in the later section. Additionally, after mutation strategy, the variables that search out of border should be amended according to the boundary.

3.2.3. Crossover

Crossover strategy is utilized to further improve the global capability of DE, which is formulated as:

$$U_{i,j}^{G} = \left\{ \begin{array}{c} X_{i,j}^{G},\ rand(0,1] \le CR\ or\ j = j_{rand} \\ V_{i,j}^{G},\ else \end{array} \right\} \tag{23}$$

where CR is the crossover rate, which is set to 0.5 in this paper, j denotes the *j*-th variable in a vector, and j_{rand} represents a random number in the range of [1, D], where D is the dimension of the problem. Specifically, D is equal to the number of design parameters, the value of which is 11 in this paper.

3.2.4. Selection

A greedy selection method is applied in DE to choose the vectors with better fitness to replace the inferior one. Based on the maximum issue of the optimization, selection strategy can be expressed as follows:

$$X_{i}^{G+1} = \left\{ \begin{array}{c} X_{i}^{G},\ \mathrm{F}(X_{i}^{G}) > \mathrm{F}(V_{i}^{G}) \\ V_{i}^{G},\ \mathrm{F}(X_{i}^{G}) < \mathrm{F}(V_{i}^{G}) \end{array} \right\} \tag{24}$$

where F indicates the fitness/objective value of the vector.

Since DE is a heuristic algorithm for random search, the search range of design parameters must be predefined. Based on the design requirements in this paper, the search range is proposed partly according to the previous literatures [14–17] and practical conditions. Search range of design parameters of SP-DLIM proposed in this paper are listed in Table 2. Notably, if you want to design a higher-power motor, the parameter value range may need to be expanded.

Table 2. Search range of design parameters of SP-DLIM.

Design Parameters	Min. Value	Max. Value	Unit
a	0.05	0.15	m
b_s/τ_s	0.3	0.5	-
d_{con}	0.5	1.5	mm
g	10	30	mm
d	4	10	mm
s	0.1	0.5	-
Jc	3	6	A/mm^2
f_1	1	200	Hz
p	3	10	-
q	1	3	-
Nz	10	100	-

3.3. Process of the Optimal Design

Overall, the optimization framework of the SP-DLIM proposed in this paper can be divided into two layers. The outer layer is the algorithm, which provides the variable design parameters. The inner layer is the mathematical model of SP-DLIM. Evaluation is a bridge connecting the inner and outer layers, which brings the parameters provided by the outer layer into the mathematical model in inner layer for calculation to obtain the corresponding output characteristics and objective function values. Afterwards, the calculation results of the inner layer are fed back to the outer layer, allowing better parameters with better objective function values to be used as exemplars for other parameters to learn. The detailed steps are as follows:

For the outer layer, first, DE algorithm initializes the population within the proposed search range. The population contains several different vectors, and each vector is composed of 11 design variables within the search range. Then, every vector is evaluated by the established mathematical model of SP-DLIM, and a corresponding objective function

value is obtained. Better vectors are saved and learned as exemplars, and different vectors with different qualities exchange the information to search the more potential vectors.

For the inner layer, generally, the calculation is carried out with the rated voltage and the given rated thrust. However, to simplify the calculation, in this paper, the primary current is calculated first as the current density and the wire size is chosen as design variables. Moreover, the number of turns per phase is also given as inputs. Therefore, all the parameters in the equivalent circuit can be calculated directly, and the output and the required line voltage can be obtained. Further, the following constraints are defined to make the design practical:

$$B_t \leq 1.2 \text{ T} \tag{25}$$

$$\frac{g-d}{2} \leq 3 \text{ mm} \tag{26}$$

$$F_{em} \leq F_{desired} \tag{27}$$

$$U_1 \leq 500 \text{ V} \tag{28}$$

Note that if a set of parameters cannot satisfy all the constraints listed above, the corresponding objective function is set to -1, which will be eliminated in the evolution process. The proposed optimization process of a SP-DLIM is illustrated as Figure 4.

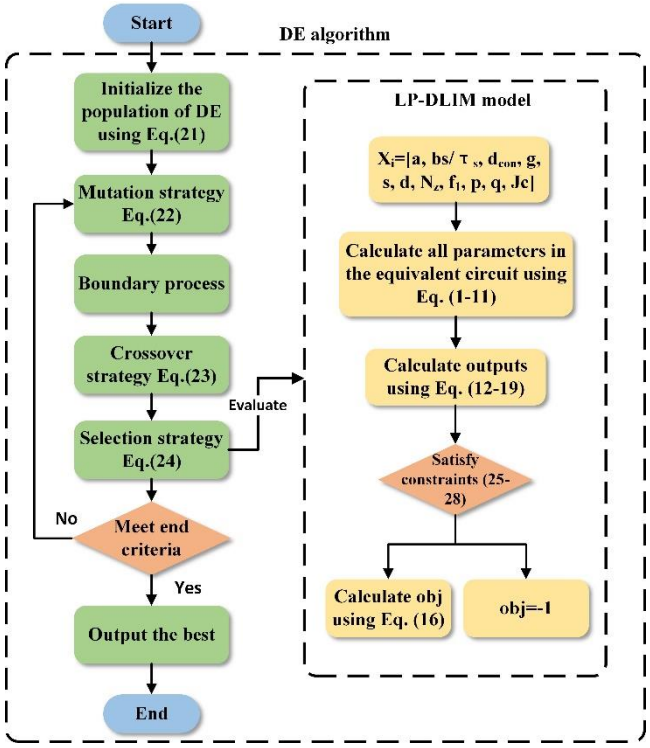

Figure 4. SP-DLIM design optimization process.

4. Optimal Results and FEM validation

This chapter gives the optimal parameters of the SP-DLIM, and finite element method (FEM) is employed to verify the validation of the proposed optimization method.

4.1. Optimal Results

4.1.1. Operating Rules of DE Algorithm

For details of DE algorithm, please refer to literature [24]. For DE, the end criteria are determined by the maximum number of evaluations (maxFEs), as other heuristic algorithms [25]. Further, the maxFEs is calculated by $10^4 \times$ D, where D is number of dimensions of the problem [25]. In this paper, D = 11. Therefore, maxFEs is set as 1.1×10^5.

What's more, DE is executed for 51 independent times to examine the stability. Further, other pivotal parameters of DE are as follows:

- Crossover rate is 0.5;
- Scaling factor is set as a randomly distributed number for every individual;
- Population size is set as 50.

4.1.2. Optimal Results

The experiment is implemented with MATLAB R2020a on a PC with i7-10750H CPU @ 2.60GHz. The average and the best results of 51 independent runs are shown in the Table 3. Note that the listed optimal results are selected from the set of parameters with the best objective function value in 51 independent runs. Moreover, the average and best output values in 51 independent runs are exhibited in table to examine the reliability and stability of the algorithm. Precisely, for output characteristics, 'Mean' and 'Best' indicate the average and best value of the specific output in 51 independent runs, respectively. While 'Optimal' value is provided by the parameters with best objective function value. Further, the table suggests that the mean, best and optimal values are not much different, which proves that the optimization results are steady and reliable.

Table 3. Optimal design results of SP-DLIM by DE within 51 independent runs.

Type	Parameters	Unit	Optimal Results	
Design parameters	Primary stack width (a)	mm	85.8	
	Slot width/slot pitch (b_s/τ_s)	-	0.5	
	Conductor diameter (d_{con})	mm	1.5	
	Number of turns per slot (N_z)	-	52	
	Number of slots/pole/phase (q)	-	3	
	Number of pole pairs (p)	-	3	
	Supply power frequency (f_1)	Hz	76.18	
	Primary current density (J_c)	A/m^2	6×10^6	
	Slip (s)	-	0.24	
	Secondary thickness (d)	mm	4	
	Air gap length (g)	mm	10	
Equivalent circuit parameters	Slot width (b_s)	mm	6	
	Tooth width (t_s)	mm	6	
	Pole pitch (τ)	m	0.108	
	Line voltage (U_1)	V	500	
	Primary turns per phase (N_{ph})	-	468	
	Primary current (I_1)	A	21.21	
	Phase winding resistance (R_1)	Ω	0.73	
	Phase winding leakage reactance (X_1)	mH	12.5	
	Slot height (h_1)	mm	21.7	
	Goodness factor (G)	-	10.1	
Output characteristics	Efficiency (η)	%	Mean Best/Optimal	71.87 73.29/71.74
	Power factor (pf)	%	Mean Best/Optimal	61.01 63.16/61.11
	Thrust (Fem)	$N \times 10^3$	Mean Best/Optimal	1.12 1.18/1.12
	Tooth weight	kg	Mean Best/Optimal	9.51 9.25/9.45
	Objective function value	-	Mean Best/Optimal	51.53 52.66/51.91

4.1.3. Comparison Results between DE, PSO, and GA

In order to test the performance of DE algorithm on the SP-DLIM optimization problem, we fairly compare DE with two other classical optimization algorithms, genetic

algorithm (GA) [26] and particle swarm optimization (PSO) [27]. Each algorithm is independently executed for 51 times, and the max fitness evaluation number of each algorithm is same. Further, DE with different parameters F and CR is investigated. Figures and Table 4 show the optimization results for 51 independent runs of each algorithm. The first rank of each indicator is highlighted in bold and shading background.

Table 4. Comparison of DE, PSO and GA within 51 independent runs.

OFV	DE	PSO	GA	F = 0.2	F = 0.3	F = 0.4	F = 0.5	F = 0.6	F = 0.7	F = 0.8	F = 0.9
Successful rate	100%	64.71%	43.14%	94%	**100%**	**100%**	47.06%	**100%**	**100%**	**100%**	**100%**
Best	**52.66**	50.89	48.86	53.13	52.24	52.15	51.76	51.91	52.66	52.66	**53.14**
Worst	**39.81**	24.40	30.16	40.40	39.81	49.84	24.36	**51.91**	**51.91**	**51.91**	**51.91**
mean	**51.68**	43.59	40.33	50.77	51.17	51.74	42.46	51.91	51.94	**52.00**	**52.00**
Std	**1.70**	7.35	4.14	1.99	1.87	0.59	7.33	**0**	0.15	0.24	0.29
OFV	**F = 1**	**CR = 0.1**	**CR = 0.2**	**CR = 0.3**	**CR = 0.4**	**CR = 0.5**	**CR = 0.6**	**CR = 0.7**	**CR = 0.8**	**CR = 0.9**	**CR = 1**
Successful rate	**100%**	98%	98%	**100%**	**100%**	**100%**	98%	**100%**	**100%**	**100%**	94%
Best	53.12	52.25	52.31	52.64	52.66	52.66	52.91	**53.14**	**53.14**	**53.14**	**53.14**
Worst	48.33	49.02	51.70	51.81	**51.91**	**51.91**	39.81	**51.91**	39.81	39.81	33.47
mean	51.99	51.4	51.91	51.97	51.95	51.95	51.72	51.96	50.78	50.35	47.35
Std	0.58	0.84	0.11	0.19	0.18	0.18	1.71	0.22	3.89	4.54	6.43

DE used CR = 0.5 in each generation and F = rand for each solution vector. F = [0.2, 1] denotes the parameter F in DE is set as [0.2, 1] with a constant CR value 0.5; similarly, CR = [0.1-1] denotes the parameter CR in DE is set as [0.1, 1] with a constant F = 0.7. OFV denotes the objective function value. From the table, in 51 runs, DE can provide solutions that satisfying all constrains, while PSO and GA obtained the successful solutions 33 and 22 times, with successful rate 64.71% and 43.14%, respectively. Moreover, with F > 0.6 and CR is approximately 0.5, DE could provide steady and accurate solutions in SP-DLIM optimization problems.

From Figure 5, the first three subfigures show the convergence of DE, PSO, and GA, respectively. The last subfigure suggests the distribution of the optimal OFV provided by DE, PSO and GA in 51 runs. DE obtain the best solutions and the fastest convergence speed compared to GA and PSO. What's more, DE can steadily acquire the best results. The improved boxplot vividly shows the distribution of the optimization results. In details, the white point represents the quartile of the data group. The OFV result provided by DE optimization is very concentrated around 51, therefore, the optimal result of DE is better and more stable.

According to above analysis, DE algorithm has better performance in design optimization of DLIMs.

4.2. 2-D transient FEM Simulation Results

Optimization results of the SP-DLIM are verified by ANSYS 2-D transient finite element method. Notably, since urban rail transit runs at a steady speed most of the time, this paper considers the optimization problem of the motor in steady-state operation, control methods and transient calculations including starting and braking characteristics are not within the scope of the study. To simplify the model, following assumptions are made:

Starting and braking conditions are not taken into account, the motor runs smoothly at a constant speed.

In order to simplify the model, we can fix the mover and set the excitation frequency to the slip frequency (i.e., slip*frequency) to simulate the relative velocity between the traveling wave magnetic field and the mover [16].

What's more, the three-phase current asymmetry is ignored; therefore, the simulation is executed under the excitation of sinusoidal current source:

$$I_A = \sqrt{2} I_1 \sin(s\omega t) \tag{29}$$

$$I_B = \sqrt{2} I_1 \sin(s\omega t - \frac{2}{3}\pi) \tag{30}$$

$$I_C = \sqrt{2} I_1 \sin(s\omega t - \frac{4}{3}\pi) \tag{31}$$

Design parameters can be seen in Table 3. Importantly, the total number of finite elements is appropriate 240 thousand, and part of the mesh plot is shown in Figure 6.

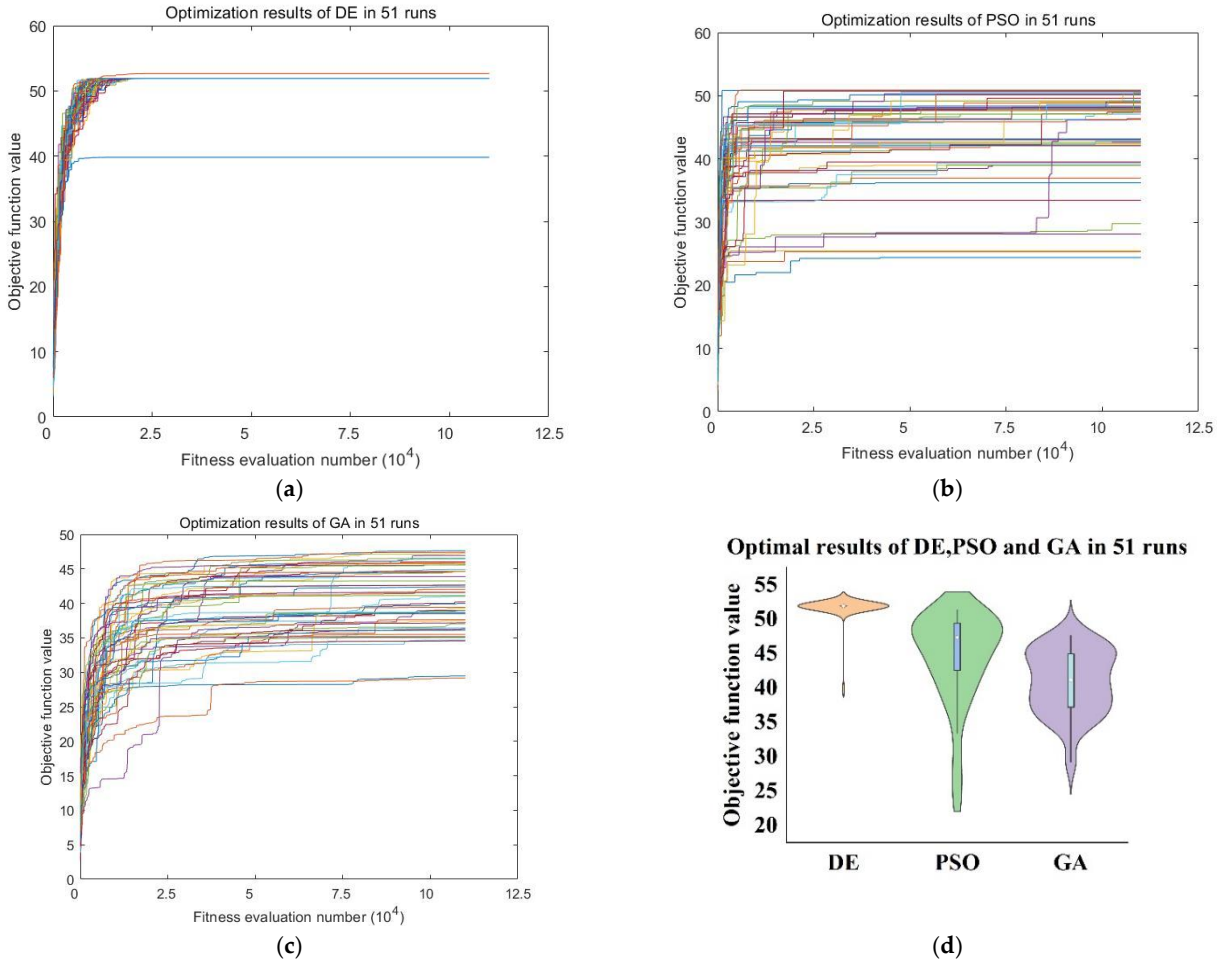

Figure 5. Convergence and statistics analysis of DE, PSO and GA within 50 runs. (**a**–**c**) show the convergence of DE, PSO, and GA, respectively. (**d**) suggests the distribution of the optimal OFV provided by DE, PSO and GA in 51 runs.

Furthermore, the magnetic flux density and flux lines in one period are shown in the figure below, where t is the current time and T represents the period.

Figure 7 above show the movement of the traveling wave magnetic field and the magnitude of the flux density. It can be concluded that the tooth flux density value is about 0.6 T, and the value of flux density in the iron core is less than 1.2 T, thus there is no over-saturation phenomenon, which certificates the rationality of the design. What's more, the average thrust of the optimally designed motor in steady state operation is 1.08 kN, shown in Figure 8, which is consistent with the calculated value (1.12 kN). The thrust in y direction (approximately 0 N) also reflects that the double-sided structure can effectively offset the normal force. Moreover, some of the key characteristics of the analytical calculation optimal results and 2-D transient FEM are listed in Table 5. It should be noted that RMS value of phase current is set as 21.5 A in 2-D FEM, and the efficiency of FEM is calculated by Equation (14), where the value must be provided by FEM results. From the comparison results, the validation of the optimization method is verified. However,

due to the incalculable phase input voltage in current-excited 2-D FEM, the power factor is not available.

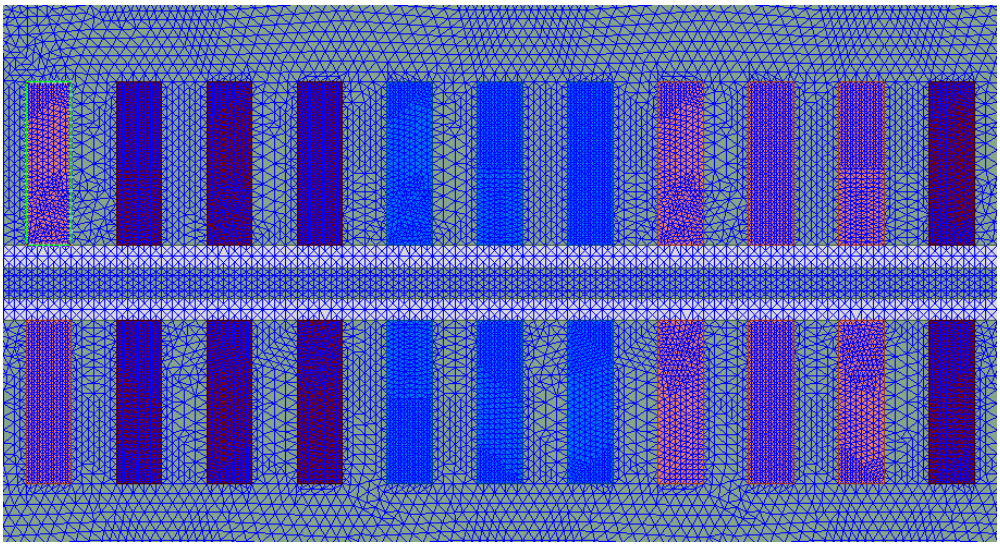

Figure 6. Part of the mesh plot of the optimal SP-DLIM.

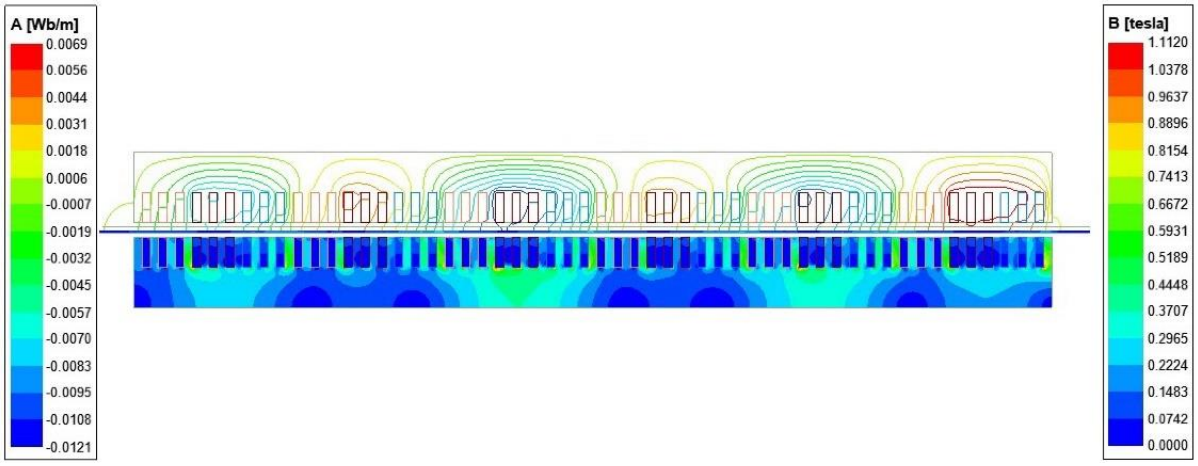

(**a**)

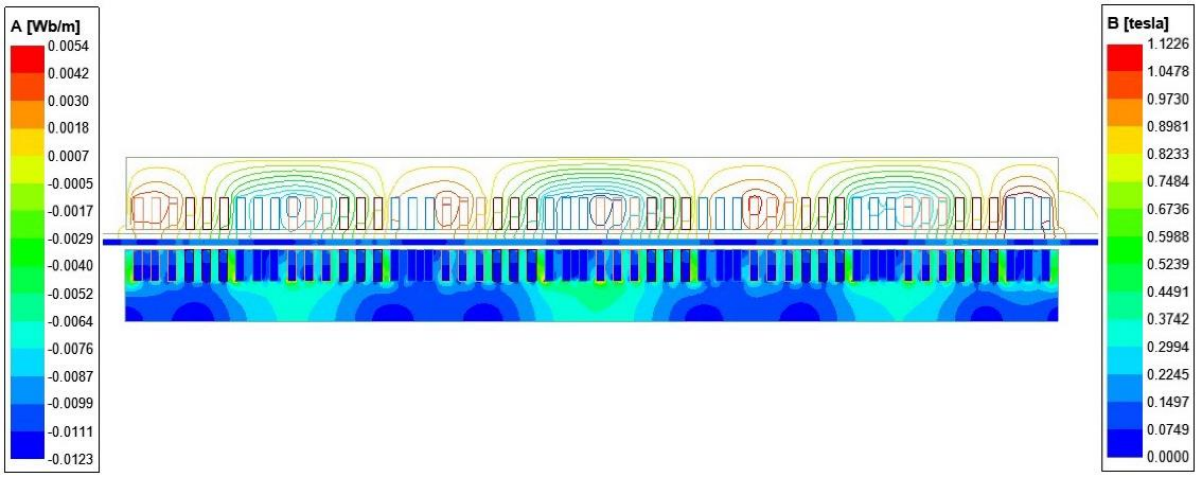

(**b**)

Figure 7. *Cont.*

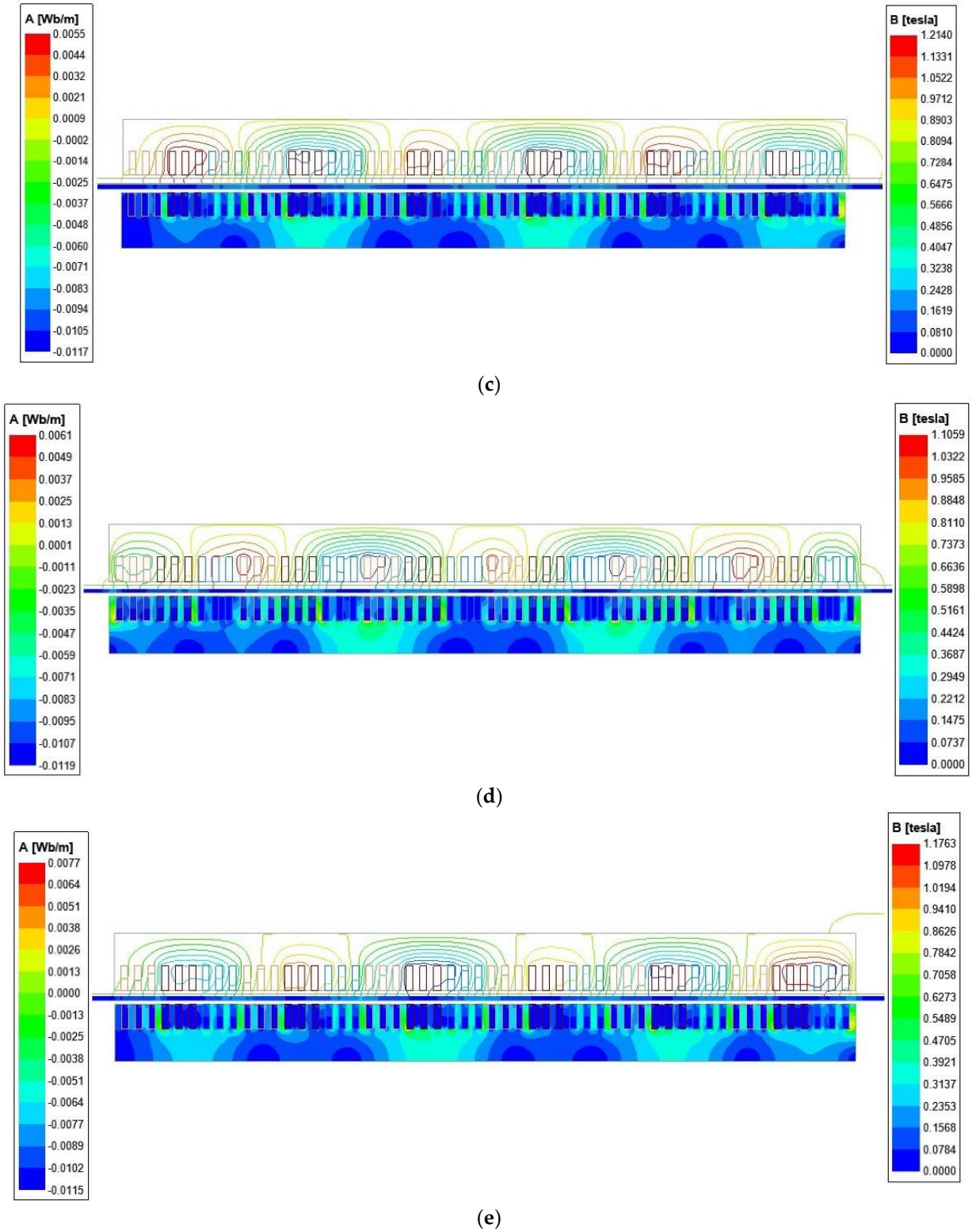

Figure 7. Distribution of flux lines and flux density when SP-DLIM is running in a steady state at (**a**) t = 0; (**b**) t = 0.25 T; (**c**) t = 0.5 T; (**d**) t = 0.75 T; (**e**) t = T. (**a**) Flux lines and flux density distribution at t = 0. (**b**) Flux lines and flux density distribution at t = 0.25 T. (**c**) Flux lines and flux density distribution at t = 0.5 T. (**d**) Flux lines and flux density distribution at t = 0.75 T. (**e**) Flux lines and flux density distribution at t = T.

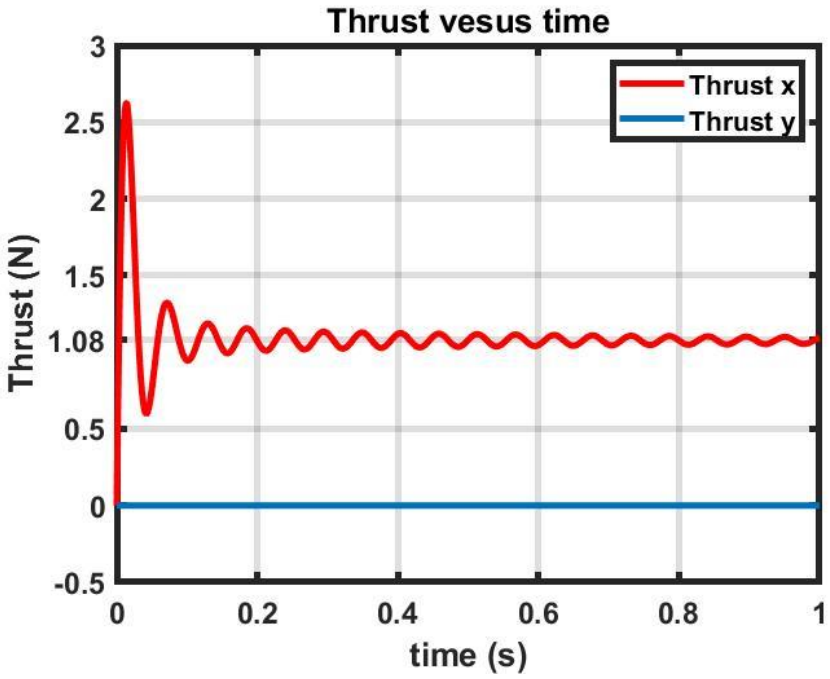

Figure 8. The time curve of thrust acting in the xdirection and y-direction of the mover.

Table 5. Some of the key characteristics of analytical calculation and 2-D transient FEM.

Characteristics	Optimal Results	FEM	Relative Error
Phase current	21.21 A	21.5 A	1.3%
Thrust	1117 N	1076 kN	3.8%
Efficiency	71.84%	71.09%	1.1%

5. Discussion

The above optimization results are in good agreement with the 2-D FEM results, which proved the accuracy of the optimization method proposed in this paper. However, for rail transit, its thrust requirement may be much greater than 1000 N. This may be improved by changing the wire size to increase the current and increasing basic mechanical size. But for high-power electrical machines, more constraints should be considered at design and analysis, which increased the difficulty of optimal design. Additionally, we utilize slip frequency in 2-D FEM to simulate relative motion between primary core and mover, which may not completely match the actual situation. These may become the content of future research.

Although the research in this article has the above shortcomings, the proposed optimization ideas can provide guidance for optimal design of various electrical equipment, especially when the rated current is required and input voltage must be constrained.

6. Conclusions

This paper proposed an optimal design method for the short primary double-sided linear induction motor (SP-DLIM) for urban rail transient. The equivalent circuit model of SP-DLIM is established, and the output characteristics are derived. Moreover, the parameters search range and constraints of the optimal design is proposed, and the objective function is defined. Additionally, the differential evolutionary (DE) algorithm is employed to optimize the design. Finally, the 2-D transient finite element method is used to verify the validation of the optimal results. The proposed optimization method may provide reference for various optimization problems for DLIMs and electrical vehicles (EVs) applied in nowadays smart grids.

Author Contributions: Conceptualization, J.Z. and Y.X.; methodology, H.W.; software, H.X.; validation, S.Y. and H.W.; formal analysis, J.Z.; investigation, Y.X.; resources, J.Z.; data curation, H.W.; writing—original draft preparation, H.W.; writing—review and editing, S.Y. and Y.X.; visualization, H.W.; supervision, J.Z. and Y.X.; project administration, J.Z. and Y.X.; funding acquisition, J.Z. All authors have read and agreed to the published version of the manuscript.

Funding: This research received no external funding.

Institutional Review Board Statement: Not applicable.

Informed Consent Statement: Not applicable.

Conflicts of Interest: The authors declare no conflict of interest.

References

1. Lu, J.; Ma, W. Research on End Effect of Linear Induction Machine for High-Speed Industrial Transportation. *IEEE Trans. Plasma Sci.* **2011**, *39*, 116–120. [CrossRef]
2. Nonaka, S.; Higuchi, T. Elements of linear induction motor design for urban transit. *IEEE Trans. Magn.* **1987**, *23*, 3002–3004. [CrossRef]
3. Xu, W.; Zhu, J.; Tan, L.; Guo, Y.; Wang, S.; Wang, Y. Optimal design of a linear induction motor applied in transportation. In Proceedings of the 2009 IEEE International Conference on Industrial Technology, Churchill, VIC, Australia, 10–13 February 2009; pp. 1–6.
4. Solomin, V.A.; Solomin, A.V.; Zamshina, L.L. Mathematical Modeling of Currents in Secondary Element of Linear Induction Motor with Transverse Magnetic Flux for Magnetic-Levitation Transport. In Proceedings of the 2019 International Conference on Industrial Engineering, Applications and Manufacturing (ICIEAM), Sochi, Russia, 25–29 March 2019; pp. 1–6. [CrossRef]
5. Ruihua, Z.; Yumei, D.; Yaohua, L.; Ke, W.; Huamin, Q. Experimental research of linear induction motor for urban mass transit. In Proceedings of the 2010 International Conference on Electrical Machines and Systems, Incheon, Korea, 10–13 October 2010; pp. 1524–1527.
6. Cho, H.T.; Liu, Y.C.; Kim, K.A. Short-Primary Linear Induction Motor Modeling with End Effects for Electric Transportation Systems. In Proceedings of the 2018 International Symposium on Computer, Consumer and Control (IS3C), Taichung, Taiwan, 6–8 December 2018; pp. 338–341. [CrossRef]
7. Lv, G.; Zhou, T.; Zeng, D.; Liu, Z. Influence of Secondary Constructions on Transverse Forces of Linear Induction Motors in Curve Rails for Urban Rail Transit. *IEEE Trans. Ind. Electron.* **2019**, *66*, 4231–4239. [CrossRef]
8. Abdollahi, S.E.; Mirzayee, M.; Mirsalim, M. Design and Analysis of a Double-Sided Linear Induction Motor for Transportation. *IEEE Trans. Magn.* **2015**, *51*, 1–7. [CrossRef]
9. Long, X. *The Theory and Electromagnetic Design Method of Linear Induction Motors*; Science Press: Beijing, China, 2006.
10. Boldea, I. *Linear Electric Machines, Drives, and MAGLEVs Handbook*; CRC Press: Boca Raton, FL, USA, 2013.
11. Duncan, J. Linear induction motor-equivalent circuit model. *Proc. IEEE* **1983**, *130*, 51–57.
12. Osawa, S.; Wada, M.; Karita, M.; Ebihara, D.; Yokoi, T. Light-weight type linear induction motor and its characteristics. *IEEE Trans. Magn.* **1992**, *28*, 3003–3005. [CrossRef]
13. Laporte, B.; Takorabet, N.; Vinsard, G. An approach to optimize winding design in linear induction motors. *IEEE Trans. Magn.* **1997**, *33*, 1844–1847. [CrossRef]
14. Hassanpour Isfahani, A.; Ebrahimi, B.M.; Lesani, H. Design optimization of a low speed single-sided linear induction motor for improved efficiency and powerfactor. *IEEE Trans. Magn.* **2008**, *44*, 266–272. [CrossRef]
15. Lucas, C.; Nasiri-Gheidari, Z.; Tootoonchian, F. Application of an imperialist competitive algorithm to design of linear induction motor. *Energy Convers. Manag.* **2010**, *51*, 1407–1411. [CrossRef]
16. Bazghaleh, A.Z.; Naghashan, M.R.; Meshkatoddini, M.R. Optimum design of single sided linear induction motors for improved motor performance. *IEEE Trans. Magn.* **2010**, *46*, 3939–3947. [CrossRef]
17. Bazghaleh AZare Naghashan, M.R.; Meshkatoddini, M.R.; Mahmoudimanesh, H. Optimum design of high speed single-sided linear induction motor to obtain best performance. In Proceedings of the SPEEDAM 2010, Pisa, Italy, 14–16 June 2010.
18. Zhao, J.; Zhang, W.; Fang, J.; Yang, Z.; Zheng, Q.T.; Liu, Y. Design of HTS Linear Induction Motor using GA and the Finite Element Method. In Proceedings of the 2010 5th IEEE Conference on Industrial Electronics and Applications, Taichung, Taiwan, 15–17 June 2010. [CrossRef]
19. Shiri, A.; Shoulaie, A. End effect braking force reduction in high-speed single-sided linear induction machine. *Energy Convers. Manag.* **2012**, *61*, 43–50. [CrossRef]
20. Xu, W.; Zhu, J.G.; Zhang, Y.; Li, Y.; Wang, Y.; Guo, Y. An Improved Equivalent Circuit Model of a Single-Sided Linear Induction Motor. *IEEE Trans. Veh. Technol.* **2010**, *59*, 2277–2289. [CrossRef]
21. Lv, G.; Zeng, D.; Zhou, T. An Advanced Equivalent Circuit Model for Linear Induction Motors. *IEEE Trans. Ind. Electron.* **2018**, *65*, 7495–7503. [CrossRef]
22. Yang, T.; Zhou, L.; Li, L. Influence of Design Parameters on End Effect in Long Primary Double-Sided Linear Induction Motor. *IEEE Trans. Plasma Sci.* **2011**, *39*, 192–197. [CrossRef]

23. Yang, T.; Zhou, L.; Li, L. Performance calculation for double-sided linear induction motor with short secondary. In Proceedings of the 2008 International Conference on Electrical Machines and Systems, Wuhan, China, 17–20 October 2008; pp. 3478–3483.
24. Das, S.; Suganthan, P.N. Differential Evolution: A Survey of the State-of-the-Art. *IEEE Trans. Evol. Comput.* **2011**, *15*, 4–31. [CrossRef]
25. Guohua, W.; Rammohan, M.; Suganthan, P. *Problem Definitions and Evaluation Criteria for the CEC 2017 Competition and Special Session on Constrained Single Objective Real-Parameter Optimization*; Nanyang Technological Universityr: Singapore, 2016.
26. Davis, L. *Handbook of Genetic Algorithms*; Van Nostrand Reinhold: New York, NY, USA, 1990.
27. Poli, R.; Kennedy, J.; Blackwell, T.M. Particle swarm optimization. *Swarm Intell.* **2007**, *1*, 33–57. [CrossRef]